Scattering off two oscillating disks: Dilute chaos

P. K. Papachristou and F. K. Diakonos
Department of Physics, University of Athens, GR-15771, Athens, Greece

V. Constantoudis
Institute of Microelectronics (IMEL), NCSR "Demokritos," P. O. Box 60228, Aghia Paraskevi, Attiki, Greece 15310
and Physics Department, National Technical University, Athens, Greece

P. Schmelcher
Theoretische Chemie, Physikalisch-Chemisches Institut, Universität Heidelberg, INF 229, D-69120 Heidelberg, Germany
and Physikalisches Institut, Universität Heidelberg, Philosophenweg 12, D-69120 Heidelberg, Germany

L. Benet
Centro de Ciencias Fisicas, UNAM, Apdo. Postal 48-3, 62251 Cuernavaca, Mexico
(Received 6 July 2004; published 19 November 2004)

We investigate the role of the unstable periodic orbits and their manifolds in the dynamics of a time-dependent two-dimensional scattering system. As a prototype we use two oscillating disks on the plane with the oscillation axes forming an angle θ. The phase space of the system is five dimensional and it possesses a variety of families of unstable periodic orbits (UPOs) with intersecting manifolds. We perform numerical experiments to probe the structure of distinct scattering functions, in one and two dimensions, near the location of the UPOs. We find that the corresponding manifolds occur only in a very particular and localized way in the high-dimensional phase space. As a consequence the underlying fractal structure is ubiquitous only in higher-dimensional, e.g., two-dimensional, scattering functions. Both two-dimensional and one-dimensional scattering functions are dominated by seemingly infinite sequences of discontinuities characterized by small values of the magnitude of the projectile's outgoing velocity. These peaks accumulate toward the phase-space locations of the UPOs, with a rate which monotonically depends on the corresponding instability exponent. They represent the intersections of the set of the initial conditions with invariant sets of larger dimensionality embedded in the phase space of the system, which are not directly related with the UPOs. We adopt the term "dilute chaos" to characterize these phenomenological aspects of the scattering dynamics.

DOI: 10.1103/PhysRevE.70.056215 PACS number(s): 05.45.Jn, 05.45.Pq

I. INTRODUCTION

Since the dawn of modern Hamiltonian classical mechanics a lot of work has been devoted to the study of the nonlinear dynamics of low-dimensional systems [1]. Among an impressive number of interesting questions considered by many authors, the role of time dependence of the interaction potentials was also investigated. Time dependence increases the dimension of the phase space by destroying typically the energy conservation. For bound systems, even for one degree of freedom (DOF), this leads in general to chaotic behavior expressed through the appearance of exponential sensitivity to the initial conditions [2–4]. For open systems the influence of time dependence of the scattering potential has been essentially considered only in one DOF periodically kicked Hamiltonian systems (yielding a two-DOF map), mainly due to the difficulties caused by the increase of the dimensionality of the phase space [5,6]. A detailed comprehension of scattering processes has been achieved for time-independent systems of two DOFs; in this case, the effective phase space is three dimensional. In these systems, chaotic scattering manifests through the existence of homoclinic and heteroclinic intersections of the manifolds of the unstable periodic orbits (UPOs), yielding a fractal arrangement of singularities in the scattering functions [7–11]. Notice that the converse is not true [12]. If the scattering functions present a finite number of singularities the scattering is considered as regular.

Moving on to systems with higher-dimensional phase space, the extension of the definition and properties of chaotic scattering is not straightforward. The role of the UPOs is less clear, since they may be too dilute in phase space. Yet, it has been shown that other invariant objects may exist in phase space with manifolds possessing sufficiently large dimensions to affect and explain the structure of the scattering functions [13–16]. In particular, we mention the occurrence of *gates* [16]. Their manifolds are invariant objects that define boundaries in phase space, just in the same way as separatrices do. The implications of such an object on scattering dynamics has been studied recently in a three-DOF system, consisting of three atoms on a plane interacting with pairwise Morse potentials [16]. The gate for this system corresponds to a specific configuration, namely, one atom resting with zero velocity infinitely far away from the other two; hence, the gate manifold is of codimension 1 in the energy surface.

The collective effect of the UPOs and their manifolds on the gate and the gate manifolds in a multidimensional scattering system remains largely an unsolved problem. The motivation of this work is to examine this effect when the multidimensionality of the phase space is caused by the time dependence of the scattering potential. In particular, we ad-

dress this problem for a system with two oscillating hard disks as scatterers. Planar scattering off hard disks represents a prototype of low-dimensional open systems. When the hard potential is time independent, the system has two DOFs and the effective phase space is three dimensional. For one or two disks the scattering process is regular due to the presence of an additional integral of motion; the corresponding scattering functions show a smooth behavior [17]. For three noncollinear disks there is no other integral besides the energy and the situation changes dramatically: The scattering functions possess a widely fluctuating form with singularities on a fractal set [18,19].

Introducing time dependence, in particular through oscillation of the hard-disk potential, leads to a five-dimensional phase space (x,y,u_x,u_y,t), where (x,y) are the coordinates on the scattering plane and (u_x,u_y) the components of the projectile's velocity. One therefore could expect naively that chaotic scattering should naturally appear, provided that the corresponding dynamics support the presence of UPOs, and connections among them. The situation is in fact more complicated [20–22]. Time dependence allows important energy transfer processes to take place between the target and the projectile. These events may lead to a large decrease of the projectile's velocity, which manifest in the scattering functions as low-velocity peaks (LVPs) [21,22]. Even in the case of one oscillating disk, where no periodic orbit is present, a set of discontinuous peaks occurs [21]. In fact, these peaks are related to the intersection of the set of initial conditions with the stable manifold of the LVPs, or gate. For the one-disk system the gate is defined as the set of stationary phase-space points satisfying $u_x=u_y=0$. As explained in [21], this set does not possess stable/unstable manifolds in a strict sense, but only marginally: There are collisions (with respect to the variation of the initial conditions) with almost vanishing outgoing projectile velocity, yielding a LVP. The corresponding scattering functions show an accumulation of discontinuous LVPs toward $|\vec{u}|=0$.

Due to the lack of UPOs in the one-disk system it is not possible to explore the influence of the set of unstable periodic orbits on the gate and its manifolds. For this reason we consider the scattering off two oscillating disks with a nonvanishing angle between their oscillation axes. This setup allows for the presence of several families of UPOs. We perform a detailed analysis of scattering functions depending on one or two variables. We find the following among other things.

(1) The UPOs influence the structure of the manifolds of the gate, since they are accumulation points of infinite sequences of LVPs. We are able to explain this in terms of a simple one-dimensional model.

(2) The rate of accumulation is characterized by a scaling factor determined by the stability properties of the corresponding UPO.

(3) The set of LVPs, in turns, seems to separate regions in phase space, and apparently controls the existence of heteroclinic connections among the UPOs.

The outline of the paper is as follow. In Sec. II we describe our model system. In Sec. III the periodic orbits of the system are determined. In Sec. IV we present our main numerical results on the scattering functions and interpret them by focusing on the role of the periodic orbits. In Sec. V we study the interrelation between the manifolds of the UPOs and the set of LVPs. In Sec. VI we quantify the self-similarity of the scattering functions. Finally in Sec. VII we summarize our main results.

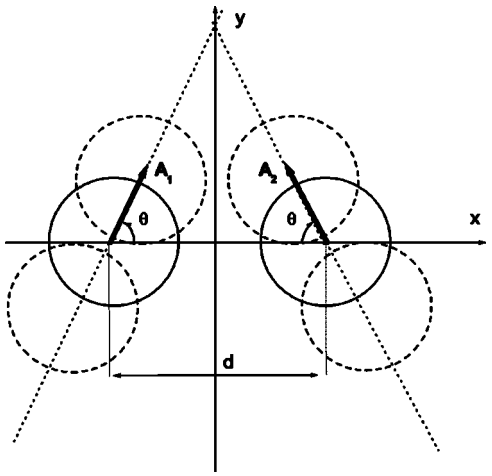

FIG. 1. The two oscillating disks on the plane. The solid circles represent the disks at their equilibrium positions, whereas the dashed ones are the disks at their extremal positions. The axes of oscillation are also shown (dotted lines).

II. THE TWO-DISK DRIVEN SCATTERING SYSTEM

The system under consideration consists of two hard disks of infinite mass harmonically oscillating on the plane, with their axes of oscillation forming angles θ and $\pi-\theta$, respectively, with the x axis. The position of the center of the disks $i=1, 2$ as a function of time is given by

$$\mathbf{x}_{Ci}(t) = \mathbf{x}_{Ci}^0 + \mathbf{A}_i \sin(\omega t + \phi_i), \tag{1}$$

where $\mathbf{x}_{Ci}^0$ is the equilibrium position of the center of the ith disk, $\mathbf{A}_i$ is its amplitude of oscillation, ω its frequency, and ϕ_i its initial phase. The potential that is felt by a particle scattered by the disks can be written as

$$V(\mathbf{x},t) = \sum_{i=1}^{2} V_0 \Theta(R_i - \|\mathbf{x} - \mathbf{x}_{Ci}(t)\|), \tag{2}$$

where R_i is the radius of the ith disk and the limit $V_0 \to \infty$ is taken. For concreteness we consider $\|\mathbf{A}_1\|=\|\mathbf{A}_2\|=A$, $\phi_1=\phi_2=\phi_0$, and $\theta=\pi/4$. We write $\mathbf{A}_1=A(\cos\theta,\sin\theta)$, $\mathbf{A}_2=A(-\cos\theta,\sin\theta)$, $\mathbf{x}_{C1}^0=(-d/2,0)$, and $\mathbf{x}_{C2}^0=(d/2,0)$, with d the distance between the centers of the disks at their equilibrium positions, as shown in Fig. 1. The positions of the centers of the disks as a function of time are therefore given by

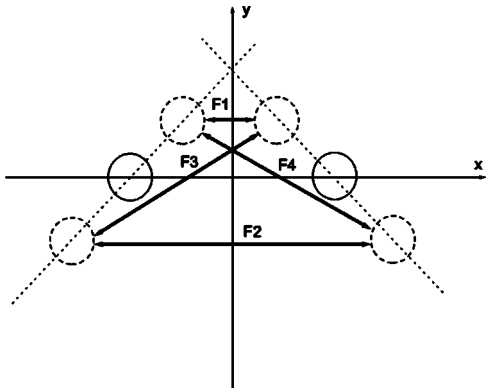

FIG. 2. The four families of energy conserving periodic orbits. The solid circles represent the disks at their equilibrium positions, whereas the dashed ones represent the disks at their extremal positions. The axes of oscillation are shown as dotted lines.

$$\mathbf{x}_{Ci}(t) = \left(\mp \frac{d}{2} \pm A \cos\theta \sin(\omega t + \phi_0) \right) \mathbf{i} + (A \sin\theta \sin(\omega t + \phi_0)) \mathbf{j}. \quad (3)$$

Here, the upper signs refer to disk 1, the lower signs to disk 2, and $\mathbf{i}, \mathbf{j}$ are unit vectors in the x, y directions, respectively. By choosing A as the length unit and $1/\omega$ as the time unit, we can introduce the dimensionless variables $\tilde{x} = x/A$ and $\tilde{t} = \omega t$. In these variables, the potential becomes $\tilde{V}_0 = V_0/(mA^2\omega^2)$, with m the mass of the scattered particle. The relevant parameters are therefore $\tilde{R} = R/A$, $\tilde{d} = d/A$, and the angle θ. From now on we shall use dimensionless variables and omit the tilde for the sake of simplicity.

In this work the values of the parameters are $R = 5$ and $d = 15$. They have been chosen such that the system exhibits a rich dynamical behavior.

III. PERIODIC ORBITS

In general, collisions can occur with stationary and nonstationary disks. Collisions with stationary disks, i.e., when the particle meets the disks at their extremal positions, conserve the energy of the particle. Collisions with nonstationary disks lead to a change in the energy of the particle, except in the case of radial collisions, i.e., when the velocity of the particle relative to the disk is radially directed.

A. Periodic orbits of constant energy

Collisions at the extremal positions of the disks yield no energy transfer, since at these positions the disks are stationary. Hence, periodic orbits colliding at these locations conserve the energy. These orbits exist and appear as discrete families; they are denoted in Fig. 2 as F1, F2, F3, and F4. F4 is the reflection symmetric image of F3 with respect to the y axis. We will refer to them as upper, lower, and diagonal families, respectively. All periodic orbits within these families possess the same projection onto position space, but differ with respect to their momenta.

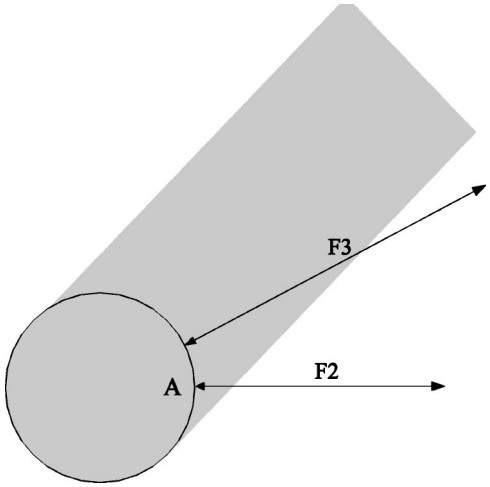

FIG. 3. Segments of the periodic orbits of the families F2 and F3 penetrating the interaction region, shown as a shaded area.

1. Upper periodic orbits

For this family, the time between successive collisions is a multiple of the period $\tau = 2\pi$ of the disks. Therefore, their period is a multiple of 2τ. Their velocities are given by

$$u_n = \frac{d - 2\cos\theta - 2R}{2\pi n} \quad (4)$$

where $n = 1, 2, \ldots$. These orbits reach the border of the interaction region, which is defined as the region where the particle can interact with the disks. There is no lower limit with respect to the magnitude of the velocity that the particle should possess in order to be on a periodic orbit. The number of periodic orbits of this family is therefore infinite.

2. Lower periodic orbits

For these periodic orbits, the time between successive collisions is again a multiple of τ and their period is a multiple of 2τ. Their velocities are given by

$$u_n = \frac{d + 2\cos\theta - 2R}{2\pi n} \quad (5)$$

where $n = 1, 2, \ldots, n_{\max}$. These orbits do enter the interaction region, as shown in Fig. 3. Consider a particle that starts off from a point A (see Fig. 3), with velocity $\mathbf{u} = u_n \mathbf{i}$, for some n. If the velocity of the particle is too small, before leaving the interaction region the particle can be scattered off successively by the same disk (at point A). That is, even if the particle has the correct velocity in order to meet the other disk at time $n\tau$, a sufficiently slow projectile will be scattered by the same disk it originated from before leaving the interaction region. Consequently, there is an upper limit $n_{\max}$ for n, which depends on the geometric parameters of the system. The value of $n_{\max}$ is approximately obtained by

$$n_{\max} \approx \begin{cases} \dfrac{d + 2\cos\theta - 2R}{2(\sqrt{R^2 - 4\sin^2\theta} + 2\cos\theta - R)}, & R \geqslant 2\tan\theta, \\ \dfrac{(d + 2\cos\theta - 2R)\arccos(1 - R/\tan\theta)}{2\pi R(1/\sin\theta - 1)}, & R < 2\tan\theta. \end{cases} \tag{6}$$

This formula is derived using the assumption that the periodic orbit n exists if the particle emitted from point A (see Fig. 3) with velocity $\mathbf{u} = u_n\mathbf{i}$ does not collide with the disk before exiting the collision region, which is shown as a shaded area in Fig. 3. A detailed derivation of these formulas as well as a deeper investigation of the dynamical behavior in terms of the parameters will be given in a future work [23]. The number of periodic orbits depends on how much the projection of the periodic orbits onto position space overlaps with the interaction region. When the equilibrium distance of the disks is large compared to the amplitude of the oscillation ($d \gg 1$) and their radius is small ($R \ll 1$), a large number of orbits exist.

3. Diagonal periodic orbits

In this case, the time between successive collisions is an odd multiple of $\tau/2$ and their period is a multiple of τ. There are two families of such orbits, related by reflection with respect to the y axis. Their velocities are given by

$$u_k = \frac{\sqrt{d^2 + 4\sin^2\theta} - 2R}{k\pi}, \tag{7}$$

where $k = 1, 3, \ldots, k_{\max}$. As in the case of the lower periodic orbits, these orbits enter the interaction region (cf. Fig. 3) and therefore there is an upper limit $k_{\max}$ of the accessible values of k. The value of $k_{\max}$ is approximately given by

$$k_{\max} \approx \begin{cases} \dfrac{\sqrt{d^2 + 4\sin^2\theta} - 2R}{\sqrt{R^2 - 4\sin^2(\theta - \Psi)} + 2\cos(\theta - \Psi) - R}, & R \geqslant 2\tan\psi, \\ \dfrac{\arccos(1 - R\tan\psi)(\sqrt{d^2 + 4\sin^2\theta} - 2R)}{\pi R(1/\cos\psi - 1)}, & R < 2\tan\psi, \end{cases} \tag{8}$$

where $\psi = \Psi + \pi/2 - \theta$, and

$$\Psi = \arctan\left(\frac{2\sin\theta}{d}\right). \tag{9}$$

B. Periodic orbits of nonconstant energy

These orbits exhibit nonradial collisions with moving disks as well as collisions with stationary disks. Consequently an exchange of energy between the disks and the particle takes place. In our system locating such orbits is a hard numerical task mainly because of their strong instability. We have found only two orbits of this kind and their reflection symmetric counterparts with respect to the y axis. In our study we have restricted our search to non-energy-conserving orbits that exhibit one collision with a disk at its extremal position.

The first orbit of this kind we have located is shown schematically in Fig. 4(a). The orbit starts at a point A of the stationary disk 2 with a velocity u_0 normal to the disk. It then collides with disk 1 at a point B while the velocity of the disk is directed downward. At this collision the particle loses energy, and since its relative velocity is directed radially, it returns toward disk 2 following the same path. It collides again with disk 2 at the point A and its velocity is reversed. It then collides again with disk 1 at the same point B, but this time it gains energy because the disk velocity is directed upward. It then returns to the point A after time 2τ with velocity u_0. Our numerical results show that this orbit is isolated in the sense that it does not appear as a member of a family. Note that the distance AB is traversed four times with two different velocities in the course of one period 2τ of the periodic orbit.

The second orbit starts at a point A of the stationary disk 2 with a velocity u_0 directed horizontally, as shown in Fig. 4(b). It then moves horizontally until it collides with the stationary disk 1 at point B. It then changes its direction, since the collision is not radial, and collides with disk 2 at point C. For this collision the velocity of the disk is directed upwards. It collides at points B and A again and then it collides with disk 1 at point D. For this collision the velocity of the disk is directed upwards. The particle then returns to point A with the same velocity u_0 it started with. This periodic orbit has period 4τ.

C. Lyapunov exponents

In the following we investigate the largest Lyapunov exponent of the periodic orbits of the system. To do this we

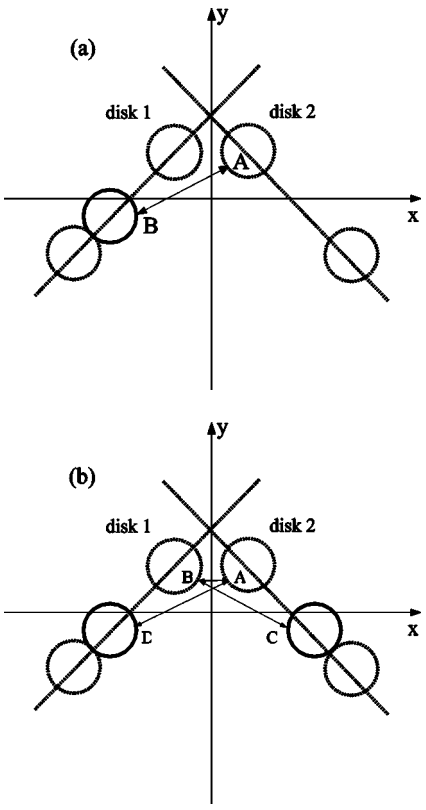

FIG. 4. Schematic representation of two non-energy-conserving periodic orbits of the system. The period of the orbit in (a) is 2τ and in (b) it is 4τ, where τ is the period of the oscillation of the disks. The extremal positions of the disks and the axes of oscillation are indicated with the dotted lines.

integrate two orbits, one is the periodic orbit and the other is an orbit with a slightly perturbed initial condition

$$\mathbf{x}(0) = \mathbf{x}_{PO}(0) + \vec{\varepsilon}_1,$$

$$\mathbf{u}(0) = \mathbf{u}_{PO}(0) + \vec{\varepsilon}_2, \tag{10}$$

where $\mathbf{x}_{PO}(0), \mathbf{u}_{PO}(0)$ correspond to the initial conditions of the periodic orbit and $\vec{\varepsilon} = (\vec{\varepsilon}_1, \vec{\varepsilon}_2)$ is a small random perturbation vector in phase space.

We calculate the largest finite time Lyapunov exponent as the slope of a straight line fitted to the curve $\ln[r(t)/|\vec{\varepsilon}|]$, where $r(t)$ is the phase-space distance between the two orbits as a function of time. Starting close enough to the periodic orbit ($|\vec{\varepsilon}| \approx 10^{-7}$) we were able to integrate the orbits for several periods, typically 15 or more. We have found that the calculated Lyapunov exponent converges well in a time less than four periods. The value of the calculated Lyapunov exponent as well as its convergence properties are practically independent of the initial position and the direction of the perturbation vector $\vec{\varepsilon}$.

The Lyapunov exponents for the upper, lower, and diagonal families are shown in Fig. 5; in the case of the upper orbits we considered the first 15 orbits. We observe that the Lyapunov exponent decreases with the period of the periodic orbit. This is intuitively expected since, as $n \to \infty$, the velocity u_n of the orbit tends to zero. The periodic orbits therefore approach the orbits for which $\mathbf{u} = \mathbf{0}$ and $\mathbf{x}$ is constant and lying at the border of the interaction region. These orbits have both Lyapunov exponents equal to zero, i.e., they are marginally unstable. We note that the value of the Lyapunov exponent for the upper and the diagonal families is very close.

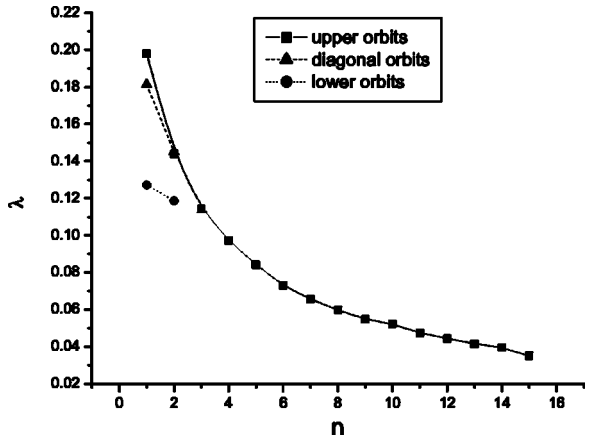

FIG. 5. Largest finite-time Lyapunov exponent for the upper (square), lower (circles), and diagonal (triangles) orbits as a function of the period.

IV. SCATTERING FUNCTIONS AND THEIR INTERPRETATION

In the numerical experiments presented below, we consider and analyze the scattering functions such as the dwell time T, and the number of collisions with the disks N. The former is defined as the time spent in the scattering region, which is a circular region of radius $R_0 \gg R$ centered at the origin that encloses the interaction region. T is equivalent to the time of flight to a detector. Mostly, we consider one-parameter scattering experiments; hence the scattering functions are given in terms of this parameter. In the scattering experiments of this section, the initial conditions are such that the particles can start arbitrarily close to a certain family of periodic orbits, and we vary only the magnitude u_0 of the initial velocity, which has a fixed direction.

A. Scattering functions probing the upper family

We choose as initial position of the particle

$$\mathbf{x}_0 = \left(-\frac{d}{2} + \cos\theta, \sin\theta \right). \tag{11}$$

The initial phase of the disks is $\phi_0 = \pi/2$. The initial velocity of the particle is directed along the positive x axis, $\mathbf{v}_0 = u_0\mathbf{i}$. Its magnitude is varied in a range where all the periodic orbits of the upper family exist. Therefore for some values of u_0 the scattered particle falls exactly onto the periodic orbits of the upper family. We compute the dwell time T and the number N of collisions with the disks in terms of the initial velocity u_0; results of this setup are shown in Fig. 6. The

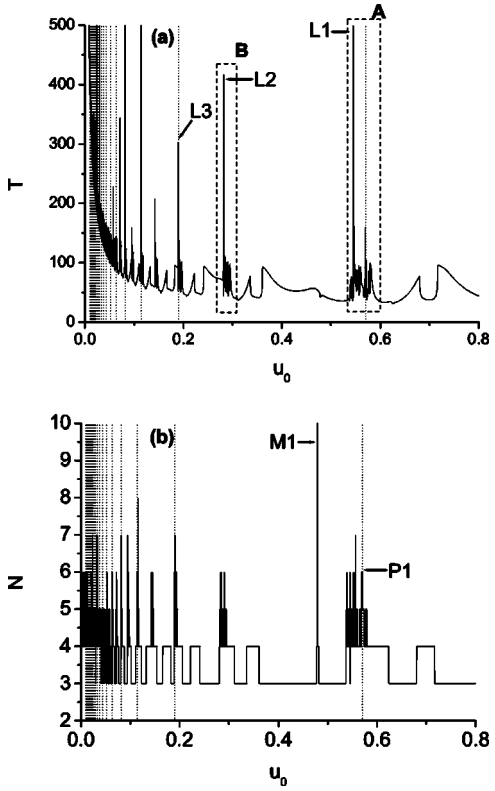

FIG. 6. Scattering functions (a) $T(u_0)$ and (b) $N(u_0)$ near the upper orbits. The locations of the periodic orbits are shown as dotted vertical lines.

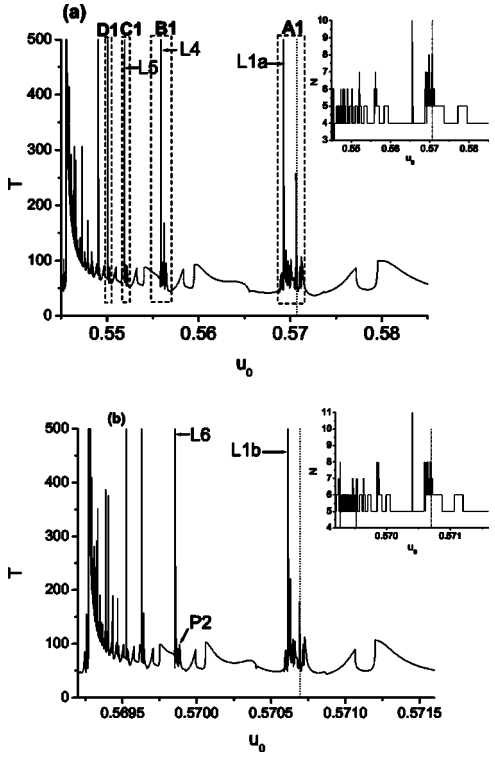

FIG. 7. (a) Magnification of the region marked as A in Fig. 6(a). (b) Magnification of the region marked as A1 in (a). In both cases, the corresponding $N(u_0)$ scattering function is shown as an inset.

locations of the periodic orbits are shown as dotted vertical lines.

The scattering functions of Fig. 6 display a rich structure of peaks around the locations of the periodic orbits. The $T(u_0)$ scattering function at the vanishing u_0 limit is dominated by a background which varies as $1/u_0$. This is due to the fact that, as $u_0 \to 0$, the particle collides for the first time with the disk at a position which tends to the extremal position of the disk. Consequently the particle traverses the orbit with a velocity that remains almost constant and equal to u_0, leading to a dwell time that grows as $1/u_0$. Periodic orbits correspond to true singularities in the scattering functions. On the left of the $n=1$ orbit, there is a prominent peak which is labeled as L1 in Fig. 6(a). Yet events leading to this peak do not display a large number of collisions. Peaks of this kind occur when the scattered particle loses a large part of its energy after a collision with a disk; we refer to such peaks as *low-velocity peaks* [21,22]. The particle then traverses a segment of its orbit (until the next collision) with a small velocity and therefore T becomes large. This specific peak is due to a loss of energy of the scattered particle after the first collision with the disks. Such peaks occur for all other $n>1$ periodic orbits and are located on values u_0 corresponding to smaller velocities. As n increases the corresponding two peaks come rapidly closer.

Peaks in the number of collisions, such as the one labeled by P1 in Fig. 6, correspond to an exact tracing of the periodic orbits by the scattered particle. These represent true singularities for both the $T(u_0)$ and $N(u_0)$ scattering functions. In Fig. 6 these peaks are relatively low due to the instability of the corresponding UPOs and the finite resolution in the calculation. We also observe that at some value of the initial velocity, there is a prominent peak in the number of collisions (labeled as M1 in Fig. 6 and no peak in T. This is due to the fact that the particle shows subsequent multiple collisions with one and the same disk for an initial velocity slightly higher than that of the disk at the instant of the first collision. These scattering events leading to peaks in the $N(u_0)$ and not in the $T(u_0)$ scattering functions have been studied in [21].

A magnification of the region marked as A in Fig. 6(a), shown in Fig. 7(a), reveals a self-similar structure; a further magnification is shown in Fig. 7(b). The peak labeled as L1a in Fig. 7(a) is analogous to the peak L1, but is due to a loss of energy after the second collision with a disk. The peak labeled as L1b in Fig. 7(b) is again similar to L1 but is due to a third collision. There is a sequence of such peaks due to the first, second, …, collisions accumulating toward the periodic orbit. This accumulation also occurs around other UPOs of this family.

The region marked as B1 in Fig. 7(a) has a structure similar to region B of Fig. 6(a). It is found that the scattered particle can approach the $n=2$ periodic orbit by starting with an initial velocity in the region B1. In the initial velocity range of Fig. 7(a) other periodic orbits of higher order n can be approached by starting with initial velocities in the regions marked as C1 ($n=3$) and D1 ($n=4$). This implies the existence of heteroclinic connections among the $n=1$ orbit and (at least) the $n=2,3,4$ periodic orbits. In the following we

will attempt to give a qualitative interpretation of this locally self-similar structure and understand its hierarchy.

B. One-dimensional representation

Since the interesting dynamics occurs close to the periodic orbits, and since on these orbits the dynamics is truly one dimensional in position space, it is meaningful and elucidating to use the following one dimensional representation. We consider the projection of the dynamics onto the axis of the periodic orbit, which in the case of the upper and lower families is the x axis. The projection of the position of the particle onto the x axis as a function of time is then represented by connected linear segments on the x-t plane. The corresponding projections of the disks are represented by two curves, which in the case of the upper orbits have the form

$$x(t) = \pm \sqrt{R^2 + \sin^2\theta(1 \mp \sin \omega t)^2} - \frac{d}{2} \pm \cos\theta \sin \omega t, \tag{12}$$

where the upper signs refer to disk 1 and the lower ones to disk 2. We emphasize that the one-dimensional representation is only approximate, and ceases to have validity when sufficient energy is transferred to the y component of the velocity of the particle. Yet the model elucidates scattering events that actually take place in the full two-oscillating-disk model.

In this one-dimensional representation, the *periodic orbits* (of the upper family) are represented by lines connecting the minima of the upper curve with the maxima of the lower curve as shown in Fig. 8(a). *Low-velocity peaks* occur when orbits encounter one of the disk's curves almost tangentially. The velocity after the collision is then small and such that the particle can escape the interaction region without colliding with the same disk twice [21,22]. After the collision, the line that represents the trajectory of the particle is almost parallel to the x axis.

Close to any initial velocity u_i that corresponds to a periodic orbit of order i, there is a velocity $u^*_{i(1)}$ that leads to a LVP immediately after the first collision. This velocity is smaller than that of the periodic orbit, $u^*_{i(1)} < u_i$. We refer to the associated peaks in the scattering functions as *primary low-velocity peaks*. The initial velocity $u^*_{i(1)}$ that leads to a LVP is in the range

$$u_t < u_{fs} < u^*_{i(1)} < u_i,$$

where u_t is the initial velocity that the particle must have in order to collide with the disk "tangentially" and u_{fs} is the initial velocity that leads to a full stop of the particle after the first collision; see Fig. 8(b). We denote by u_D the derivative of the curve that describes the disk motion (in this case the x component of the disk velocity) at the instant of the collision; then $u_t = u_D$ and $u_{fs} = 2u_D$. As i increases, both u_i and u_{fs} decrease; therefore the difference $u_i - u^*_{1(1)}$ also decreases. This means that the collisions leading to a primary LVP occur closer and closer to the extremal point (at which the periodic orbit collides with the disk and $u_D = 0$) as the period of the orbit increases. In Fig. 8(b), these events (ordered with decreasing initial velocity) are illustrated in the one-dimensional representation: (a) The periodic orbit (solid line) of velocity u_i; (b) a LVP (dotted line) corresponding to a collision after which the particle has just the energy to escape from the interaction region without colliding with a disk; (c) a full stop of the particle (dashed line) of velocity $2u_D$ (this event does not correspond to a LVP since the particle is still in the interaction region and will collide with a disk in a time interval of the order of the period of the oscillation); (d) event (dash-dotted line) when the particle has a velocity u_D equal to the disk velocity at the point of the collision.

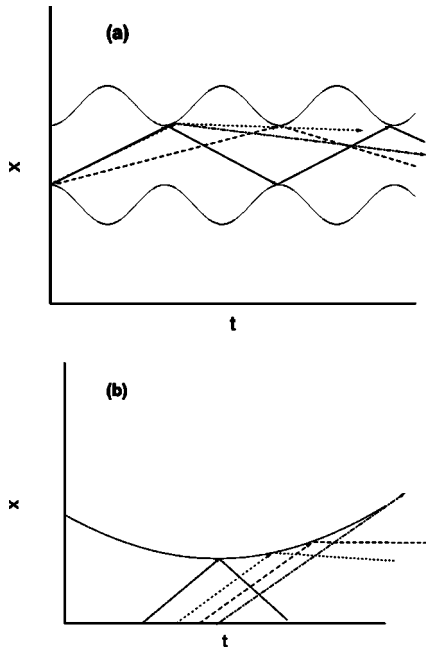

FIG. 8. (a) One-dimensional representation of the periodic orbits $n=1$ (solid line), $n=2$ (dashed line), and a primary LVP (dotted line). An orbit with $u_0 > u^*_{i(1)}$ is shown (dash-dotted line). (b) Enlargement of a region of (a): periodic orbit (solid line), LVP (dotted line), and a full stop of the particle (dashed line). The dash-dotted line corresponds to an event where the particle encounters the disk "tangentially."

After the first collision, the interval of initial velocities $\Delta u_0 = [u^*_{1(1)}, u_1]$ will spread to a much wider one, Δu_1. The same is true for $[u^*_{2(1)}, u_2]$, $[u^*_{3(1)}, u_3]$, …, defined by periodic orbits of higher order [see Fig. 9(a)]. This spread of the initial velocity interval makes accessible a large sequence of events after the first collision. Consequently, in the range $[u^*_{1(1)}, u_1]$ of initial velocities, other LVPs can occur, which are due to the second, third, etc., collisions. The initial velocities that lead to these peaks are denoted as $u^*_{1(2)}$, $u^*_{1(3)}$, …, respectively. Starting with an initial velocity $u^*_{1(2)}$ in $[u^*_{1(1)}, u_1]$, the particle can follow the periodic orbit one collision more, and exhibit a LVP after the second collision [see Fig. 9(b)]. Therefore, the same spread of the velocities mentioned above occurs also with initial velocities in the range $[u^*_{1(2)}, u_1]$ but is due to the second collision. Since in this

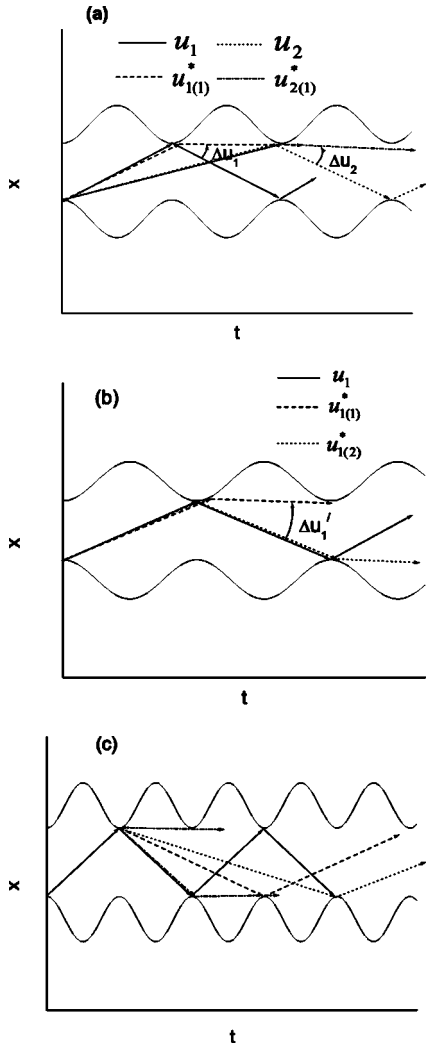

FIG. 9. (a) Illustration of the spread Δu_1 and Δu_2 of velocities after the first collision, when the initial velocity is in the interval $[u^*_{1(1)}, u_1]$ or $[u^*_{2(1)}, u_2]$. (b) Periodic orbit $n=1$ (solid line), and LVPs obtained after the first collision (dashed line) and the second collision (dotted line). (c) Events with initial velocities in the interval $[u^*_{1(1)}, u^*_{1(2)}]$. Approximate tracing of the $n=2$ periodic orbit (dashed line); a LVP after the second collision (dotted line); $n=1$ periodic orbit (solid line); and events corresponding to $u^*_{1(1)}$ and $u^*_{1(2)}$ (dash-dotted lines).

one-dimensional representation this argument holds for an arbitrary number of collisions, there is an infinite sequence $u^*_{1(1)}$, $u^*_{1(2)}$,… of LVPs accumulating toward the periodic orbit $u^*_{1(\infty)}=u_1$. An analogous representation of the whole structure is therefore contained between $u^*_{1(i)}$ and u_1. This explains the self-similar structure observed in Figs. 6 and 7. The same construction holds around other periodic orbits: For every n there is a sequence $u^*_{n(1)}$, $u^*_{n(2)}$,… of LVPs due to the first, second,… collisions accumulating towards u_n.

Starting off with initial velocities in the interval $[u^*_{1(1)}, u^*_{1(2)}]$ leads, after the first collision, to a velocity spread $\Delta u_1'$ illustrated in Fig. 9(b). The following events are then accessible. (a) Secondary LVPs: There is a sequence of

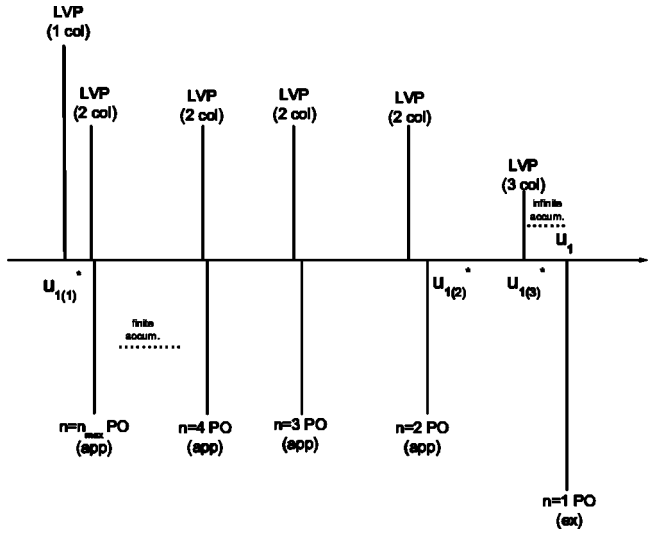

FIG. 10. Location and hierarchical arrangement of LVPs and events that correspond to approximate tracing of periodic orbits (PO app), located between $u^*_{1(1)}$ and u_1. The sequence of $u^*_{1(1)}$, $u^*_{1(2)}$, … accumulating toward the periodic orbit u_1 is also shown.

LVPs, all due to the second collision, between the initial velocities $u^*_{1(1)}$ and $u^*_{1(2)}$. They occur when the velocity of the particle after the first collision is such that the second collision [with the lower curve that describes the disk motion; see Fig. 9(c)] is almost tangent. The sequence of these peaks is not infinite, since the particle can collide with the same disk if the velocity after the first collision is small enough. (b) Approximate tracing of periodic orbits: In the same range of initial velocities, there is also a sequence of peaks which correspond to an approximate tracing of some periodic orbits of the family. They occur when the velocity of the particle after the first collision is such that the second collision is at a maximum of the lower curve [see Fig. 9(c)]. This sequence is also not infinite: The velocity after the first collision that corresponds to a LVP cannot be arbitrarily close to zero, i.e., no orbits of arbitrarily high periods can be traced.

These events occur alternatingly with varying initial velocity u_0. In Fig. 10 the hierarchy of the structure around the $n=1$ periodic orbit is schematically illustrated. The horizontal axis represents the initial velocities and the location of LVPs is shown with vertical lines above this axis. The location of the $n=1$ periodic orbit as well as the events that lead to approximate tracing of periodic orbits are shown with vertical lines below the axis. The same description carries over for all orbits of the upper family.

In terms of the one-dimensional representation, we turn now to analyze other aspects of the scattering functions (Figs. 6 and 7) for the upper orbits. In Fig. 11(a), the one-dimensional representation of the processes belonging to the peaks labeled as L1, L2, L3 of Fig. 6 is shown. These peaks are primary LVPs due to the first collision, occurring close to the $n=1,2,3$ periodic orbits in u_0 space, respectively. Their initial velocities correspond to $u^*_{1(1)}$, $u^*_{1(2)}$, and $u^*_{1(3)}$ respectively. The magnification shown in Fig. 7 displays the self-similar structure between $u^*_{1(1)}$ (peak L1) and u_1. In that range, there exists a velocity which leads to a prominent

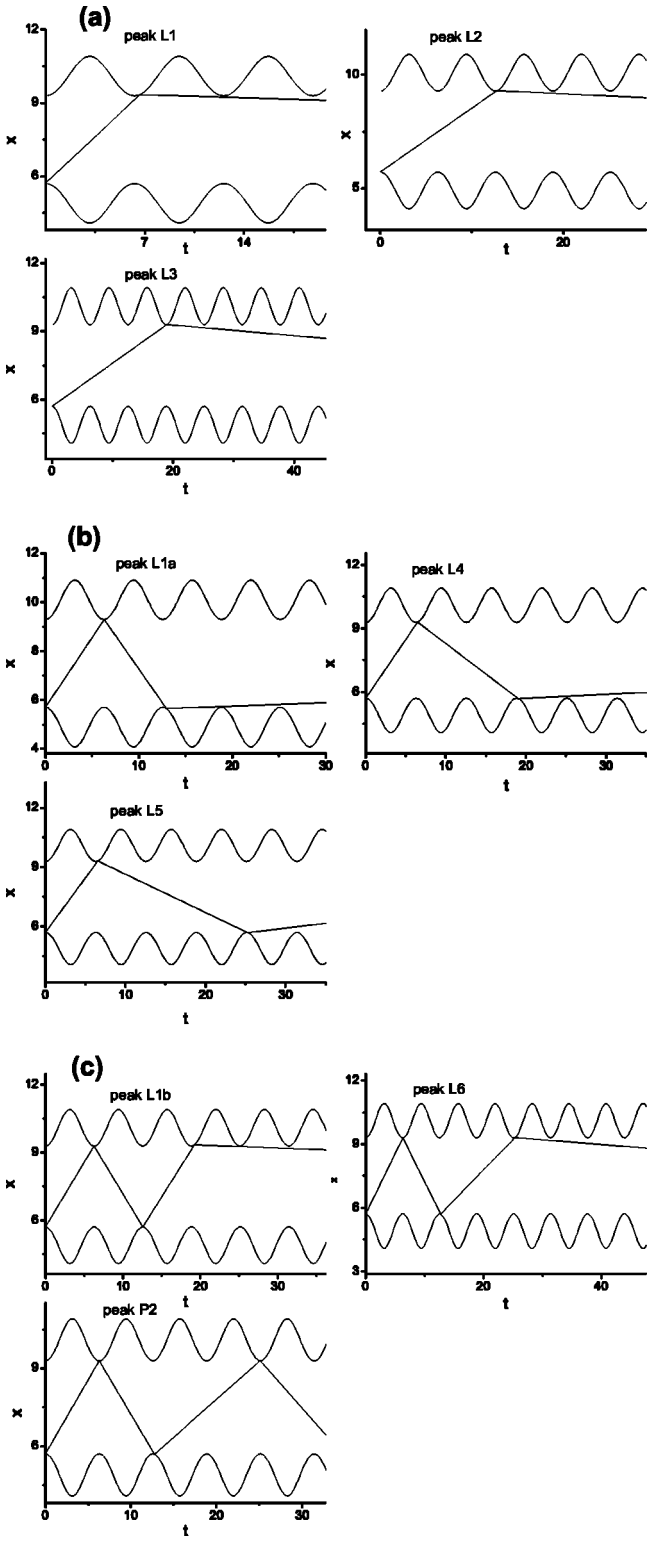

FIG. 11. One-dimensional representation of the processes near the upper family of periodic orbits. (a) Peaks labeled L1, L2, L3 in Fig. 6; (b) L1a, L4, L5 of Fig. 7(a); and (c) L1b, L6, P2 of Fig. 7(b).

LVP, labeled as L1a, close to the $n=1$ periodic orbit. As can be seen from its one-dimensional representation, this peak is ascribed to the second collision and its initial velocity corresponds to $u^*_{1(2)}$. Between $u^*_{1(1)}$ (peak L1) and $u^*_{1(2)}$ (peak L1a), there exists a sequence of LVPs due to the second collision (peaks L4 and L5) as well as a structure reminiscent of that around the $n=2,3,\ldots,n_{\max}$ periodic orbits of Fig. 6. This occurs because these orbits can be approximately traced with initial velocities in that range. The one-dimensional representation of the events belonging to the peaks labeled as L1a, L4, L5 in Fig. 7(a) is shown in Fig. 11(b). The magnification in Fig. 7(b) [region A1 of Fig. 7(a)] reveals the self-similar structure in the range $[u^*_{1(2)},u_1]$ (peak L1a, and the vertical dotted line). The prominent LVP labeled L1b is due to the third collision, and its initial velocity corresponds to $u^*_{1(3)}$. In the range $[u^*_{1(2)},u^*_{1(3)}]$ (peak L1a and peak L1b) there is again a sequence of LVPs such as L6, which are due to the third collision, and there are approximate tracings of periodic orbits, such as the peak labeled P2. The one-dimensional representation of the latter events is shown in Fig. 11(c).

We recall that the preceding description of the one-dimensional representation can only be taken over up to a certain development level of the scattering functions of the full planar oscillating two-disk system. Interestingly, the one-dimensional representation described above introduces a symbolic sequence to characterize the scattering events. We emphasize that such symbolic dynamics requires symbols assigned to the LVPs to fully describe the dynamics. This is, the invariant set *must* also include the LVPs.

C. Scattering functions probing the lower family

In this case, we use as initial position

$$\mathbf{x}_0=\left(-\frac{d}{2}-\cos\theta,-\sin\theta\right). \tag{13}$$

The initial phase of the disks is fixed to $\phi_0=3\pi/2$, and the initial velocity is directed along the positive x axis, $\mathbf{v}_0=u_0\mathbf{i}$. Its magnitude is varied in a range where periodic orbits exist; therefore for some values of u_0 the scattered particle falls exactly onto the periodic orbits of the lower family.

In Fig. 12(a) we present $T(u_0)$. Note that in this configuration only two orbits of the lower family exist. Around each periodic orbit, a rich structure is observed. In analogy to the upper family, we notice the appearance of LVPs and the self-similarity of the arrangement of peaks, as shown by the successive magnifications around the $n=1$ periodic orbit plotted in Figs. 12(b) and 12(c). However, in contrast to the upper family, our numerical results suggest that in this case a periodic orbit cannot be reached or approximately traced by starting off with initial conditions in the neighborhood of another one. This implies that there are no heteroclinic connections among different periodic orbits of this family. This impediment is due to the fact that the periodic orbits collide with the disks deep inside the interaction region. In terms of the one-dimensional representation, the periodic orbits occur colliding on the minima of the lower curve and on the maxima of the upper curve (Fig. 13). The nature of the peaks as well as their accumulation toward the periodic orbits can be explained using the same arguments as for the upper family. We turn to describe the origin of the peaks labeled in Fig. 12(a), using the same notation as for the upper orbits.

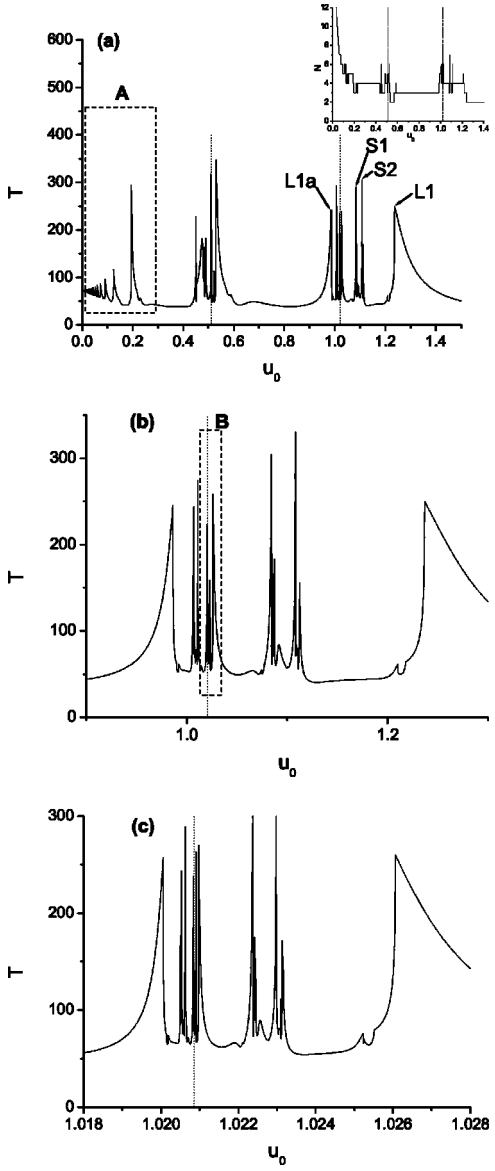

FIG. 12. (a) The $T(u_0)$ scattering function for the lower family; $N(u_0)$ is shown in the same range of u_0 in the inset. The locations of the periodic orbits are shown with dotted vertical lines. (b) Magnification of $T(u_0)$ around the $n=1$ periodic orbit; (c) magnification of the region marked as B in (b).

At the value u_1 of the initial velocity the particle moves on the $n=1$ periodic orbit leading to a singularity in the $T(u_0)$ plot. Due to the finiteness of the resolution and the instability of the orbit, this singularity appears as a relatively small peak. There is an initial velocity $u^*_{1(1)} > u_1$ for which a LVP occurs after the first collision. This peak is labeled as L1 in Fig. 12(a). The one-dimensional representation of this event is shown in Fig. 13(a). From this figure we notice that, after the collision with the disk, the particle "penetrates" the curve that describes the motion of the disk. After that collision, the velocity of the particle has an important y component, which is due to the fact that $u^*_{1(1)} - u_1$ is much larger than in the case of the upper orbits [cf. Figs. 13(a) and 7(a)]. As for the upper family, a similar peak can occur by starting closer to the periodic orbit and following it for one more collision. This corresponds to the initial velocity $u^*_{1(2)} < u_1$ and leads to the peak labeled as L1a in Fig. 12(a). The sequence $u^*_{1(1)}$, $u^*_{1(2)}$, … accumulates toward u_1 alternately: $u^*_{1(1)}$, $u^*_{1(3)}$, … are larger than u_1 whereas $u^*_{1(2)}$, $u^*_{1(4)}$, … are smaller. In Fig. 13(b), the one-dimensional representation of the trajectory corresponding to the initial velocity $u^*_{1(3)}$ is shown. This alternating behavior is due to the fact that the periodic orbits are inverse hyperbolic; in terms of the one-dimensional representation the periodic orbits alternate collisions at the minima of the lower curve and at the maxima of the upper one, which describe the motion of the disks. Around the LVPs of the scattering functions there is no additional structure, because of the important transfer of velocity to the y component, which favors the escape and prevents the appearance of additional structures. The range of initial velocities $[u^*_{1(3)}, u^*_{1(1)}]$ leads to a large spread of velocities after the first collision, denoted as Δu in Fig. 13(b). The latter makes two "secondary" LVPs accessible, namely, those labeled as S1 and S2 in Fig. 12(a). Their one-dimensional representation is shown in Fig. 13(c). Only two such peaks exist. This is due to the fact that, if a trajectory starts off with an initial velocity larger than that of peak S2, it will collide with disk 2 more than once, thus losing the possibility of colliding with disk 1 which would yield a low velocity after the collision. Similar peaks exist between $u^*_{1(2)}$ and $u^*_{1(4)}$ due to the second collision, between $u^*_{1(5)}$ and $u^*_{1(3)}$ due to the fourth, and so on. The hierarchy and the locations of the peaks described above are shown in Fig. 14.

The structure around the $n=2$ periodic orbit is similar. The important difference is that there are no peaks due to the second, third, … collision in the ranges $[u^*_{2(3)}, u^*_{2(1)}]$, $[u^*_{2(2)}, u^*_{2(4)}]$, …, respectively. This is a consequence of the fact that trajectories with initial velocities between u_2 and $u^*_{2(1)}$ (and $u^*_{2(2)}$) are "screened" by disk 2, experiencing a second collision with disk 2. This is illustrated in Fig. 13(d).

Finally, we note that the structures in the region marked as A in Fig. 12(a) are not related to periodic orbits but to the singularity in the number of collisions located at $u_0=0$.

A similar structure of LVPs accumulating toward the UPOs is also found in probing the diagonal family or orbits. The structures in the scattering functions can be explained using exactly the same arguments we used in the case of the upper and the lower families of orbits [24].

D. Scattering functions near the non-energy-conserving periodic orbits

We consider now scattering experiments whose initial conditions are in the neighborhood of one of the non-energy-conserving periodic orbits detected numerically. We choose as initial conditions

$$\mathbf{x} = \left(\frac{d}{2} - \cos\theta + R\cos(\pi + \theta_0), \sin\theta + R\sin(\pi + \theta_0) \right),$$

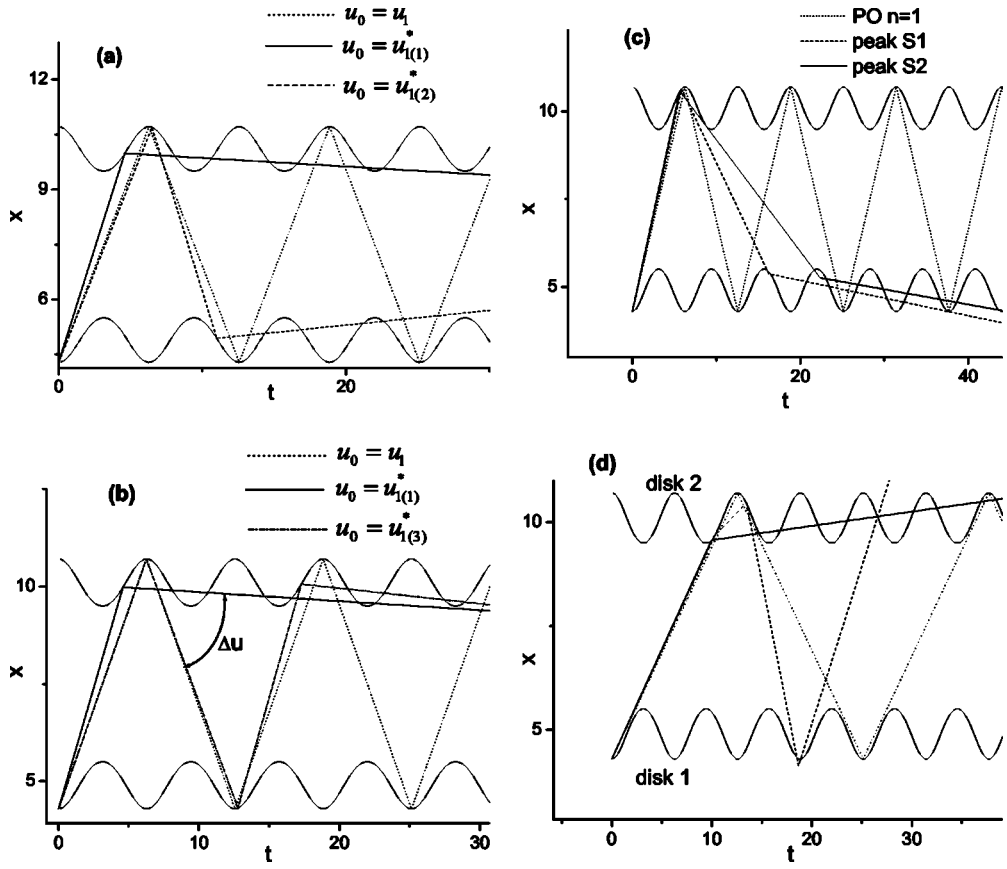

FIG. 13. One-dimensional representation of distinct trajectories near the periodic orbits of the lower family. (a) Events corresponding to u_1, $u^*_{1(1)}$, and $u^*_{1(2)}$. Clearly, the inequalities $u^*_{1(2)} < u_1 < u^*_{1(2)}$ hold. (b) Events corresponding to u_1, $u^*_{1(1)}$, and $u^*_{1(3)}$; the spread Δu is also indicated. (c) Secondary LVPs [peaks S1 and S2 of Fig. 12(a)]. (d) A trajectory with initial velocity in $[u_2, u^*_{2(1)}]$ (dashed line) experiences a second collision with disk 2 instead of one with disk 1. No other secondary LVPs besides those of (c) exist.

$$\mathbf{u} = (u_0 \cos(\pi + \theta_0), u_0 \sin(\pi + \theta_0)), \tag{14}$$

where $\theta_0 = 0.061\,335$, $\phi_0 = \pi/2$, and u_0 is varied around the value $u_0 = 1.011\,13$. Figures 15 show the results for $T(u_0)$ and $N(u_0)$, and successive magnifications are shown in Fig. 16. Remarkably, the figures display a seemingly isolated peak that corresponds to the periodic orbit. Magnifications of the scattering functions around it show that there is an accumulation of LVPs with velocities larger than that of the periodic orbit. These peaks are due to the last collision (before escape), as shown in Fig. 15(b). The absence of additional peaks in the number of collisions in these figures indicates that this orbit does not communicate with any other periodic orbit of the system, i.e., there are no homoclinic or heteroclinic connections associated with this orbit.

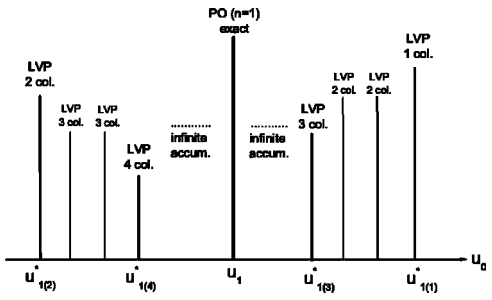

FIG. 14. Location and hierarchy of the LVPs accumulating toward the $n=1$ lower periodic orbit. The notation used is the same as in Fig. 10.

V. MANIFOLDS OF THE UPOS AND THE SET OF LVPS

In order to get a better understanding of the properties of the manifolds of the UPOs as well as their interrelations with the manifold of the gate invariant set of the system (set of LVPs) we perform two further numerical investigations.

In order to study scattering functions that explore the neighborhood of periodic orbits belonging to different families, we use a scattering setup in which both the direction and the magnitude of the initial velocity are varied by means of the parameter s. In order to construct scattering functions that probe the upper and diagonal families of orbits, the magnitude of the initial velocity is varied according to

$$u_0 = u_U + s(u_U - u_D) \tag{15}$$

where u_U is the velocity of a periodic orbit (of order n) of the upper family and u_D is the velocity of a periodic orbit (of order k) of the diagonal family. The initial velocity vector, with respect to the x axis, forms an angle φ, which is varied according to

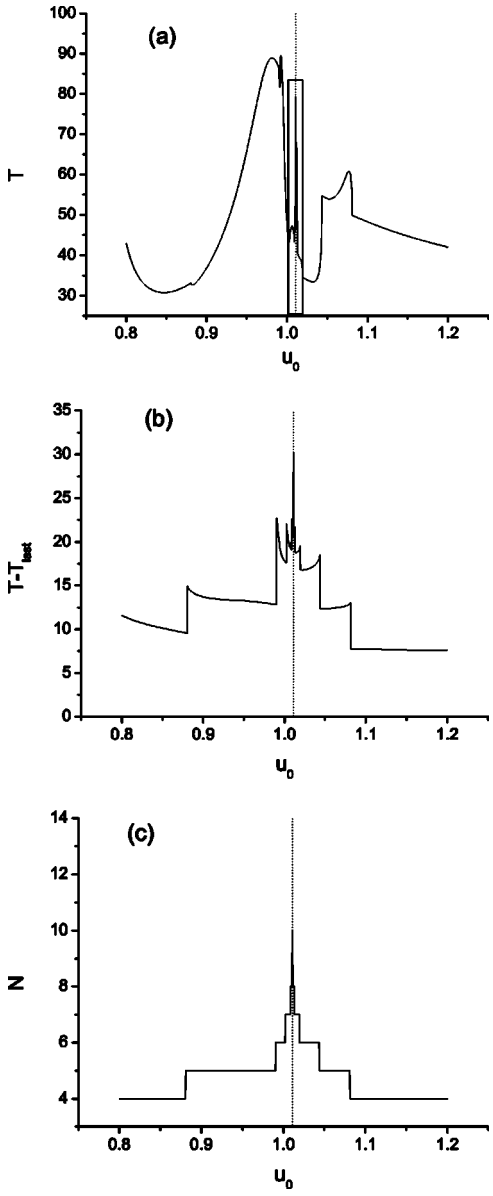

FIG. 15. Scattering functions in the neighborhood of the energy nonconserving periodic orbit: (a) Time delay T as a function of u_0; (b) subtraction of the time after the last collision from the time delay; and (c) $N(u_0)$. The location of the periodic orbit is shown with a dotted vertical line.

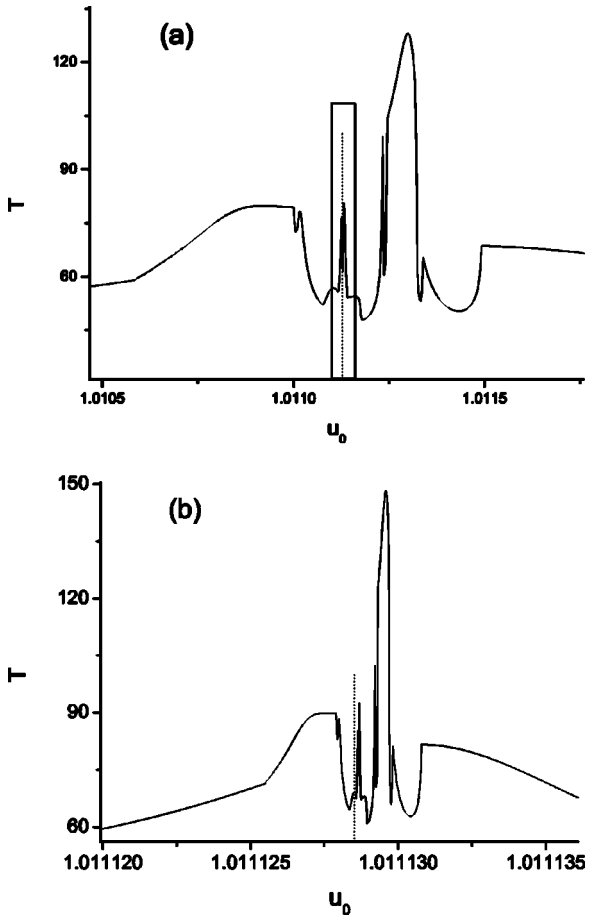

FIG. 16. Successive magnifications of the $T(u_0)$ plot of Fig. 15(a) around the periodic orbit. The location of the periodic orbit is shown with a dotted vertical line.

$$\varphi = s\Psi, \tag{16}$$

where Ψ is given by Eq. (9). Then, the initial position of the particle is

$$\mathbf{x}_0 = \left(-\frac{d}{2} + \cos\theta + R\cos\varphi, \sin\theta - R\sin\varphi \right) \tag{17}$$

and the initial phase of the disks is fixed to $\phi_0 = \pi/2$. Therefore, for $s=0$ the particle follows the nth order periodic orbit of the upper family and for $s=1$ it follows the kth order periodic orbit of the diagonal family. In the same manner we can construct a parameter to probe scattering events near the lower and diagonal families. These scattering functions will provide complementary information, as they exhibit intersections with the stable manifolds of periodic orbits of the diagonal and upper families.

In Figs. 17, the $T(s)$ and $N(s)$ scattering functions probing the $n=1$ upper ($s=0$) and the $k=2$ diagonal ($s=1$) orbits are shown. The structure around $s=0$ and $s=1$ consists of the typical accumulation of LVPs around the corresponding periodic orbits. The peak labeled as L1 is an isolated LVP occurring far from the $k=2$ diagonal periodic orbit, with a finite sequence of secondary peaks that accumulate toward it from the left. Such peaks have been encountered and studied in detail in [22]. Peaks labeled as L2 and L3 are primary LVPs located close to the periodic orbits at $s=0$ and $s=1$, respectively.

The peaks in $N(s)$, labeled as P1 and P2, correspond to tracing of periodic orbits. More specifically, it is found that peak P1 corresponds to tracing of the $k=1$ diagonal orbit and peak P2 to the second energy nonconserving orbit (of period 4τ) we found numerically. Therefore, the more complex line of initial conditions used in this scattering setup intersects the stable manifolds of periodic orbits not located at $s=0$ and $s=1$. Successive magnifications of the region around peak P2 [marked as A in Fig. 17(a)] are shown in Fig. 18. They reveal

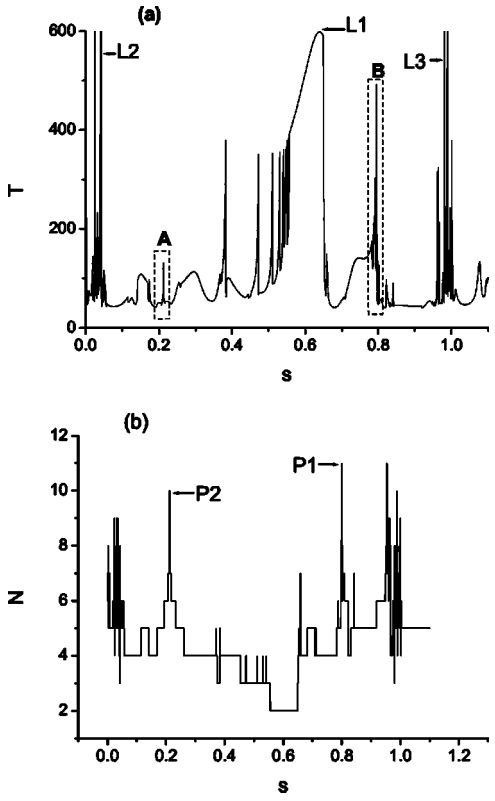

FIG. 17. (a) $T(s)$ and (b) $N(s)$ scattering functions probing the $n=1$ upper ($s=0$) and the $k=2$ diagonal ($s=1$) periodic orbits.

another isolated peak, implying the lack of homoclinic or heteroclinic connections with this periodic orbit. The same structure is revealed by successive magnifications around the region B in Fig. 17(a). This is consistent with the results probing directly these periodic orbits: no heteroclinic connections involving the diagonal (or non-energy-conserving) and upper periodic orbits are found.

Collecting our results, we have found homoclinic and heteroclinic connections between UPOs of the upper and the lower families. Yet our numerical results show that these connections occur *only* between members of the same family. This is interesting since there is no communication between periodic orbits of the upper and lower families, even though there are families of periodic orbits (i.e., the diagonal orbits) that could allow this communication.

The probing tools in the second numerical experiment are the two-dimensional scattering functions and the aim is to reveal the interrelations between the manifolds of the UPOs and those of the gate invariant set. In our system the gate invariant set [16] consists of all the points in the x-y plane outside the interaction region such that $u_x=u_y=0$, i.e., the scattered particle is at rest in a region where it can at most interact tangentially with the disks. Particles starting with a nonvanishing initial velocity outside the interaction region cannot exit the interaction region with arbitrary small or vanishing outgoing velocity. Physically, this is due to the hard-wall type of the potential. Consequently orbits can only approach this set asymptotically, in the sense of reaching very small but not arbitrarily small velocities. Therefore, the

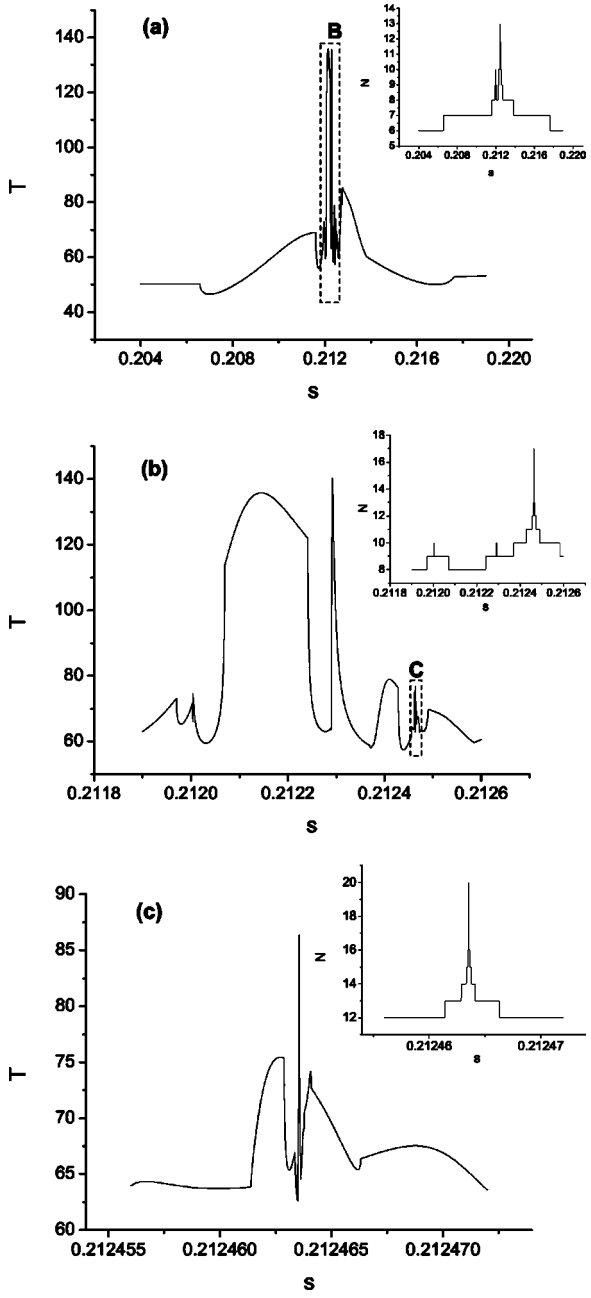

FIG. 18. (a) Magnification of $T(s)$ in the region A of Fig. 17(a); (b) magnification of the region B of (a); (c) magnification of the region C of (b). The corresponding $N(s)$ scattering functions are shown in the insets.

manifolds of the gate can be defined in a marginal sense, as the set of initial conditions leading to LVPs in the dwell-time scattering function. These initial conditions lead to orbits that, after their interaction with the disks, approach the gate as closely as possible.

A more detailed analysis of the two-dimensional scattering functions and the involved structures will be given in a future work [23]. Here we give a first record of some preliminary yet illuminating results. We choose as initial position the point

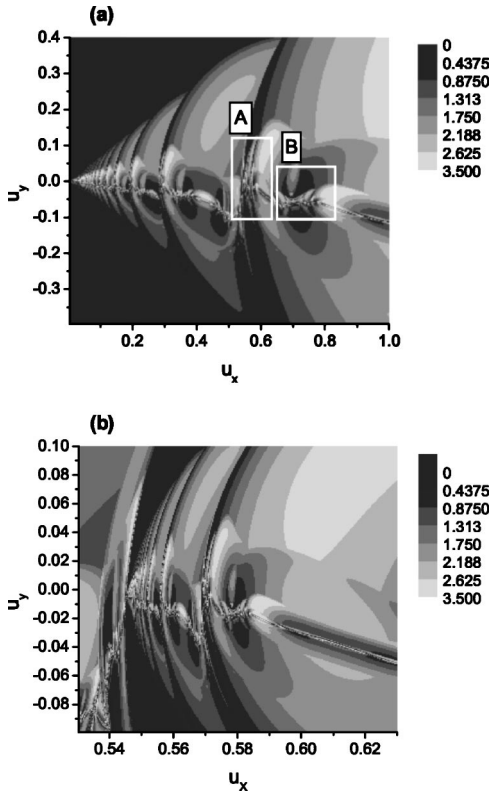

FIG. 19. (a) Outgoing velocity in terms of the components u_x and u_y of the initial velocity. In the range of initial velocities, all the periodic orbits of the upper family exist. (b) Magnification of the region A of (a). In this region the $n=1$ periodic orbit of the upper family exists.

$$\mathbf{x}_0 = \left(-\frac{d}{2} + \cos\theta, \sin\theta \right), \tag{18}$$

where $\phi_0 = \pi/2$ and the components u_x and u_y of the initial velocity are varied in a range where all periodic orbits of the upper family exist. Such orbits exist for $u_y = 0$ and u_x given by Eq. (4); concretely, $u_x \simeq 0.570$ for the $n=1$ orbit, $u_x \simeq 0.285$ for $n=2$, $u_x \simeq 0.142$ for $n=3$. The final velocity u_f of the particle after its last collision with the disks is plotted in terms of u_x and u_y. The result is shown in Fig. 19(a).

The stable manifold of the gate, as defined above, consists of initial conditions which leave the interaction region with a velocity of small magnitude. It is therefore contained in the black regions of Figs. 19. Obviously, the origin ($u_x = u_y = 0$) belongs to the gate. The figure shows the existence of points belonging to the stable manifold of the gate that accumulate towards the origin. As was mentioned before, the set of upper periodic orbits also accumulates toward the origin. Moreover, the periodic orbits are also accumulation points of the LVPs, and thus for the stable manifold of the gate. This is shown in Fig. 19(b), where a magnification of a region around the $n=1$ periodic orbit is shown.

As can be seen from the magnifications of Fig. 20, such a two-dimensional scattering function exhibits a self-similar structure. Moreover, we notice in Fig. 19 a structure which appears to be a line crossing the regions of the LVPs and

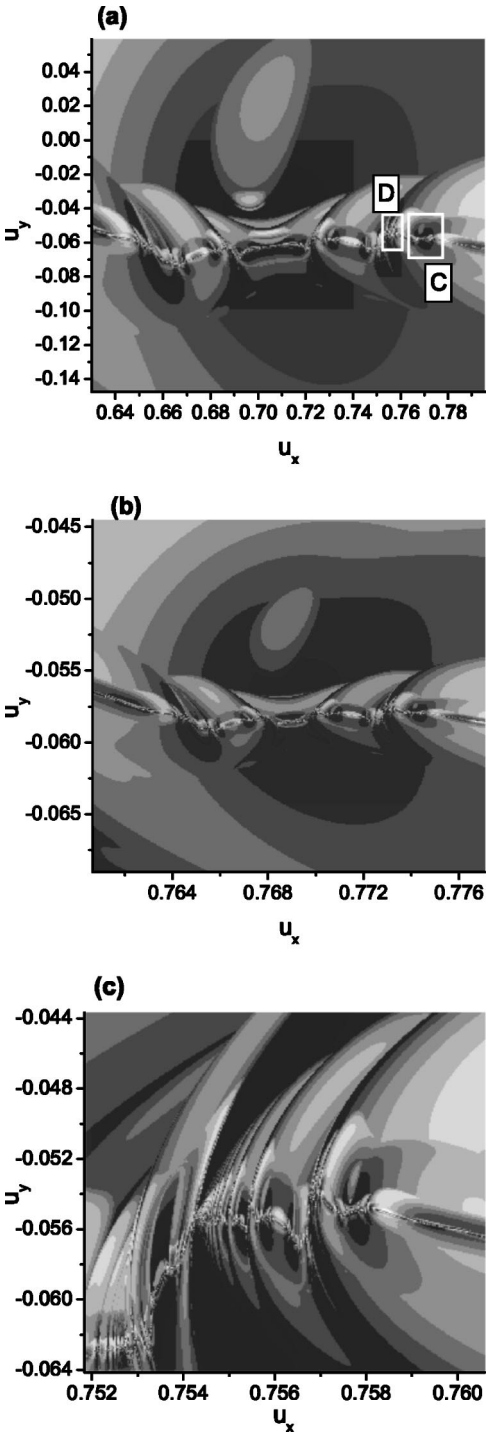

FIG. 20. (a) Magnification of the region B of Fig. 19(a); (b) magnification of the region C of (a); (c) magnification of the region D of (a).

forming a small negative angle with the axis $u_y = 0$. This structure contains phase-space points leading to orbits with many collisions, as can be seen from Fig. 21(a) where the $N(u_x, u_y)$ scattering function corresponding to Fig. 19(a) is shown. In fact, for the $\mathbf{x}_0$ of Eq. (18) these orbits approach the diagonal UPOs and therefore we can say that this structure is the intersection of the stable manifold of the diagonal orbits with the u_x-u_y plane. The stable manifold seems to be

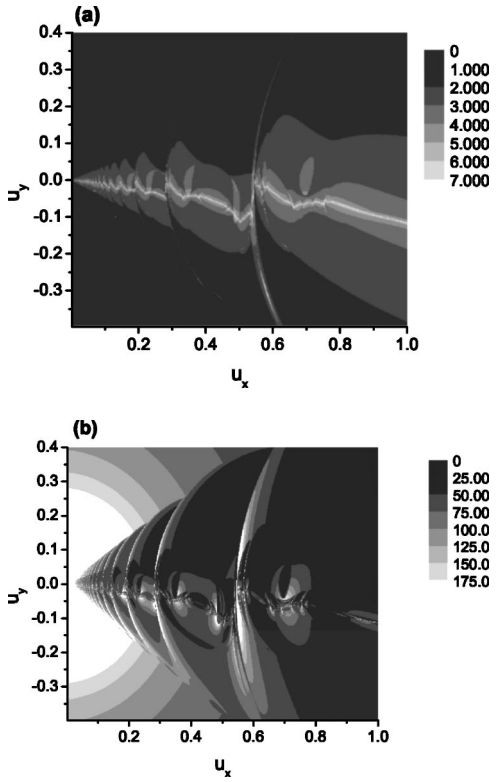

FIG. 21. (a) $N(u_x,u_y)$ scattering function corresponding to the $u_f(u_x,u_y)$ scattering function of Fig. 19; (b) $T(u_x,u_y)$ scattering function corresponding to the $u_f(u_x,u_y)$ scattering function of Fig. 19.

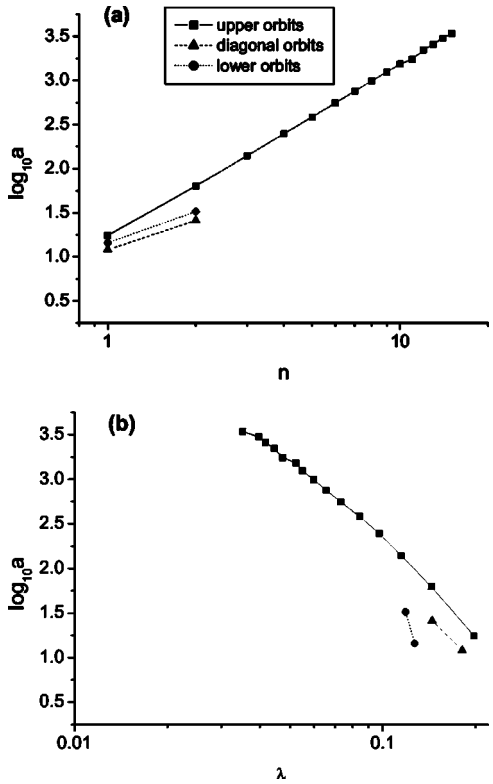

FIG. 22. (a) The value of the ratio a_n for the upper (square), lower (circles), and diagonal (triangles) orbits. (b) a_n versus the Lyapunov exponents, for the same orbits.

cut by the set of LVPs (the manifold of the gate) in almost similar parts. It has been found that these parts do not communicate in the sense that the evolution of initial conditions within such a part lead to trajectories which do not leave this part. The overall characteristics of the two-dimensional scattering functions are independent of the choice of the initial position $\mathbf{x}_0$. However the points of the apparently linear structure can occasionally belong to the manifolds of a different family of UPOs depending on the initial position $\mathbf{x}_0$. For $\mathbf{x}_0$ lying between the two disks the linear set belongs to the manifolds of the diagonal family, as already mentioned, while for $\mathbf{x}_0$ above the disks the corresponding set belongs to the stable manifold of the upper family of UPOs. Finally, for $\mathbf{x}_0$ below the disks the linear set of points belongs to the stable manifold of the UPOs of the lower family.

After that first detection of the phase-space structures of the UPOs and the gate manifold, the question that arises is their impact on the time delay of the projectile inside the scattering region. Figure 21(b) depicts the dwell-time scattering function $T(u_x,u_y)$ for the $\mathbf{x}_0$ of Eq. (18). Comparing to Fig. 21(a) we can see that the set of LVPs is clearly much more effective on the dwell time since the regions of large dwell time coincide with those of the LVPs, while the impact of the manifolds of the UPOs is apparently less important probably due to their localization in phase space and/or due to the large instability of the UPOs.

VI. QUANTIFICATION OF THE SELF-SIMILARITY OF THE SCATTERING FUNCTIONS

Let us consider the way the velocities $u^*_{n(1)}, u^*_{n(2)}, \ldots$ of the LVPs after the first, second, … collision accumulate toward the velocity u_n of a certain periodic orbit. We have numerically found that they approach u_n according to

$$\frac{|u^*_{n(1)}-u_n|}{|u^*_{n(2)}-u_n|}=\frac{|u^*_{n(2)}-u_n|}{|u^*_{n(3)}-u_n|}=\cdots=\frac{|u^*_{n(i)}-u_n|}{|u^*_{n(i+1)}-u_n|}=a_n. \quad (19)$$

Here, a_n is a constant that depends on the specific periodic orbit. It can be shown (see Appendix A) that the set of accumulating points $u^*_{n(1)}, u^*_{n(2)}, \ldots, u^*_{n(\infty)}=u_n$ has zero box-counting dimension, regardless of the value of the ratio a_n. It can also be shown (see Appendix B) that this set has local mass dimension equal to 1 around the accumulation point, independently of the specific periodic orbit in question. Therefore, we use only the value a_n to quantify the scaling properties of the structures in the scattering functions.

We have calculated the value of a_n for several orbits. The results are shown in Fig. 22(a); a_n is plotted versus the Lyapunov exponents in Fig. 22(b). It is found that the ratio a_n depends monotonically on the period of the orbit. Moreover, as can be seen from Fig. 22(a), the dependence of a_n on the index n of the periodic orbit in question, at least for the upper orbits, is to a good approximation a power law. The exponent obtained from here is 1.97. It is also found [see

Fig. 22(b)] that there is a monotonic relation between the stability of a periodic orbit and the accumulation properties of the LVPs toward it.

VII. SUMMARY AND CONCLUSIONS

In this paper, we have investigated the classical dynamics of an open system with a high-dimensional phase space, in the presence of a time-dependent zero-range potential. Specifically, we studied the scattering off two oscillating hard disks on the plane, leading to a five-dimensional phase space. We considered a general setup when the oscillation axes of the disks form an angle θ. Our main goal was twofold: (i) to determine and classify the dominant structures that characterize the scattering dynamics of the system, thereby focusing on the specific features due to the potential's time dependence, and (ii) to associate these structures with invariant sets in phase space. In particular, we were interested in clarifying the role of unstable periodic orbits in the scattering dynamics of the system.

The main tool in our investigations was the use of one- and two-dimensional scattering functions. As a first step, we have shown the existence of several families of unstable periodic orbits, whose manifolds may or may not display homoclinic or heteroclinic intersections depending on the specific periodic orbit. It turns out that the effect of homoclinic and heteroclinic connections is quite difficult to detect at the level of one-dimensional but visible at the level of two-dimensional scattering functions. These are dominated by the presence of infinite sequences of isolated peaks that accumulate toward the position of the UPOs and are characterized by a very small magnitude of the projectile's outgoing velocity; therefore they are referred to as low-velocity peaks, and result from a large energy loss of the particle after an inelastic collision with one of the disks. Our results definitely show the importance of including the set of LVPs in any attempt to describe the scattering dynamics. They form sequences organized in a hierarchical structure; this can be clearly appreciated in the time delay scattering function. Although the basic building blocks of this hierachical structure are always the invariant manifolds of the UPOs, the location and hierarchy of the LVPs depend on the particular details of the system. We were able to identify and classify the scattering events leading to the specific structure of the scattering functions using a simplified one-dimensional model. In addition, we have shown a monotonic dependence of the accumulation rate of the LVPs with respect to the stability properties of the UPO to which they accumulate.

The set of LVPs acts effectively as separatrices in the pendulum, defining boundaries in phase space. In our model system, this set allows for homoclinic and heteroclinic intersections of members of the same family of periodic orbits. The stable manifolds of such periodic orbits do reach the asymptotic (incoming) region, yielding a fractal set of singularities in the appropriate scattering functions. However, their density in phase space is quite low due to the large dimensionality of phase space; only certain two-dimensional scattering experiments detect the complexity in the system. We propose as an appropriate description of this dynamical complexity the term "dilute chaotic scattering:" It reflects the presence of homoclinic/heteroclinic connections in phase space and thus complicated scattering behavior depending on a dilute subset of initial conditions, and also the existence of dominant invariant structures (set of LVPs) which limit and regulate the influence of the UPOs. Responsible for the occurrence of dilute chaos is the instability of the UPOs and/or the extremely localized appearance [linear point set on (u_x, u_y) plane] of their stable/unstable manifolds in phase space. The occurrence of dilute chaos has also been observed using different parameter sets for the system [23,24]. In general, as the ratio d/R increases, the UPOs become more unstable and less dense in phase space. Therefore, the set of LVPs plays a more important role in the dynamics, having the same accumulation properties as those described here.

We attribute the importance of the set of LVPs in the scattering dynamics to the large dimensionality of phase space. This may be achieved by considering many degrees of freedom or by including a time-dependent potential. For conservative systems, the high dimensionality permits that the energy may be shared by the different DOFs, in particular, one or more may have no energy at all. The time dependence by itself plays an important role for the presence of LVPs. Indeed, these have been observed in time-dependent two-DOF systems which are conservative [25,26]. The time dependence of the potential, as has been noted previously, allows certain processes to display large energy loss. Again, certain regions in phase space, lying outside of the interaction region, may attain very small energy. In the cases mentioned above of time-dependent systems that become conservative, such regions in phase space have a low dimensionality because of additional constraints; in this case, only scattering experiments that are prepared without keeping the constant of motion fixed may notice them [25]. For time-dependent systems of more than two DOFs, the set of LVPs has a relatively large dimensionality. Thus, in general, scattering experiments will detect them easily. The important point to emphasize is that the set of LVPs defines invariant regions in phase space of high dimensionality, which may influence the scattering dynamics. Their manifolds may have homoclinic and heteroclinic intersections; this may explain the hierarchical structure of their accumulation toward the UPOs that we found. Moreover, they may display properties of marginal instability, like parabolic manifolds, as it is the case in our system of hard-wall potentials [21].

The above observations clearly show that the scattering situation in higher dimensions becomes qualitatively more complex. In particular, there are examples suggesting that the gate and its manifolds can take over the role of the UPOs in the basic construction of the chaotic saddle [16,26,27]. A challenging question is thus to look for a setup where the role of UPOs becomes more important again, and even dominant, in the presence of the LVPs. Moreover, a precise understanding on how the set of LVPs defines barriers in phase space for the manifolds of the UPOs remains open. Questions of this type are left for future investigations.

ACKNOWLEDGMENTS

L.B. acknowledges financial support from Projects No. IN-101603 (DGAPA-UNAM) and No. 43375-E

(CONACyT). Financial support in the framework of the IKYDA Program of the DAAD (Germany) and IKY (Greece) is gratefully acknowledged. We also thank Dr. E. Mavrommatis for helpful discussions.

APPENDIX A: BOX-COUNTING DIMENSION

We shall now calculate the box-counting dimension of a set of accumulating points. In what follows for simplicity we set u_n as the zero of the u axis of the velocities. We choose our box size to be $\varepsilon=(\ell/a)^j$ where j is an integer and ℓ is the length of the interval $[u_n, u^*_{n(1)}]$. Since the distance between u_n and $u^*_{1(j)}$ is $(\ell/a)^j$, we need one box to cover the structure between 0 and $u^*_{1(j)}$, and additional $j-1$ boxes to cover the other $j-1$ points. Therefore,

$$N(j) = 1 + (j-1) = j. \tag{A1}$$

The box-counting dimension is then

$$d_F = -\lim_{\varepsilon\to 0}\frac{\ln N(\varepsilon)}{\ln \varepsilon} = -\lim_{j\to\infty}\frac{\ln j}{\ln(\ell/a)^j} = -\frac{1}{\ln(\ell/a)}\lim_{j\to\infty}\frac{\ln j}{j} = 0. \tag{A2}$$

Consequently the set of points has zero box-counting dimension regardless of the value of the ratio a_n.

APPENDIX B: LOCAL MASS DIMENSION AROUND $u=u_n$

Here, we calculate the local mass dimension d_m of the set of points $u^*_{n(1)}, u^*_{n(2)}, \ldots$ around the accumulation point $u^*_{n(\infty)} = u_n$. The dimension d_m is defined as

$$d_m = \lim_{\varepsilon\to 0}\frac{\ln(\mu[0,\varepsilon])}{\ln \varepsilon}, \tag{B1}$$

where $\mu[0,\varepsilon]$ is the mass contained in the interval $[0,\varepsilon]$, and is given by

$$\mu[0,\varepsilon] = \int_0^{\varepsilon}\rho(u)du, \tag{B2}$$

with $\rho(u)$ being the density of points.

In our case, the distance between two successive points is

$$\begin{aligned}|u^*_{n(j+1)} - u^*_{n(j)}| &= \left|\left(\frac{\ell}{a}\right)^{j+1} - \left(\frac{\ell}{a}\right)^{j}\right| \\ &= \left(\frac{\ell}{a}\right)^{j}\left(1-\frac{\ell}{a}\right) \\ &= u^*_{n(j)}\left(1-\frac{\ell}{a}\right).\end{aligned} \tag{B3}$$

Since the density of points is analogous to the inverse of the distance, the density of points is $\rho(u)\sim 1/u$. Therefore the integral of Eq. (B2) diverges. In order to regularize the integral, we use a velocity $u^* > u_n$ to write the integral in the form

$$\mu[u^*, u^*+\varepsilon] = \int_{u^*}^{u^*+\varepsilon}\frac{1}{u}du, \tag{B4}$$

which tends to $\mu[0,\varepsilon]$ at the limit $u^*\to 0$. We will thus calculate d_m as a function of u^* and then take the limit $u^*\to 0$ if needed. Evaluating the integral of Eq. (B4) provides

$$\mu[u^*, u^*+\varepsilon] = \ln\left(1+\frac{\varepsilon}{u^*}\right). \tag{B5}$$

This yields

$$d_m = \lim_{\varepsilon\to 0}\frac{\ln[\ln(1+\varepsilon/u^*)]}{\ln \varepsilon} = 1. \tag{B6}$$

The set of points has therefore local mass dimension equal to 1 around the accumulation point, regardless of the value of the ratio a_n.

[1] A. J. Lichtenberg and M. A. Lieberman, *Regular and Stochastic Motion* (Springer, New York, 1983).
[2] M. Tabor, *Chaos and Integrability in Nonlinear Dynamics* (John Wiley & Sons, New York, 1989).
[3] E. Ott, *Chaos in Dynamical Systems* (Cambridge University Press, Cambridge, U.K., 1993).
[4] P. Gaspard, *Chaos, Scattering and Statistical Mechanics* (Cambridge University Press, Cambridge, U.K., 1998).
[5] B. Ruckerl and C. Jung, J. Phys. A **27**, 55 (1994).
[6] H. Tapia and C. Jung, Phys. Lett. A **313**, 198 (2003).
[7] B. Eckhardt, Physica D **33**, 89 (1988).
[8] C. Jung and H. J. Scholz, J. Phys. A **20**, 3607 (1988).
[9] Y. T. Lau, J. M. Finn, and E. Ott, Phys. Rev. Lett. **66**, 978 (1991).
[10] Y. C. Lai and C. Grebogi, Int. J. Bifurcation Chaos Appl. Sci. Eng. **1**, 667 (1991).
[11] E. Ott and T. Tél, Chaos **3**, 417 (1993).
[12] G. Troll, Chaos, Solitons Fractals **7**, 1929 (1996).
[13] S. Wiggins, *Chaotic Transport in Dynamical Systems* (Springer, New York, 1992).
[14] D. Beigie and S. Wiggins, Phys. Rev. A **45**, 4803 (1992).
[15] M. Toda, Phys. Rev. Lett. **74**, 2670 (1995).
[16] Z. Kovács and L. Wiesenfeld, Phys. Rev. E **63**, 056207, (2001).
[17] J. V. José, C. Rojas, and E. Saletan, Am. J. Phys. **60**, 587 (1992).
[18] B. Eckhardt, J. Phys. A **20**, 5971 (1987).
[19] P. Gaspard and S. Rice, J. Chem. Phys. **90**, 2225 (1989).
[20] A. Antillón, J. José, and T. H. Seligman, Phys. Rev. E **58**, 1780 (1998).
[21] P. K. Papachristou, F. K. Diakonos, V. Constantoudis, P. Schmelcher, and L. Benet, Phys. Lett. A **306**, 116 (2002).

[22] P. K. Papachristou, F. K. Diakonos, E. Mavrommatis, and V. Constantoudis, Phys. Rev. E **64**, 016205 (2001).
[23] P. K. Papachristou, F. K. Diakonos, V. Constantoudis, P. Schmelcher, and L. Benet (unpublished).
[24] P. K. Papachristou, Ph.D. thesis, Department of Physics, University of Athens, 2004.
[25] N. Meyer *et al.*, J. Phys. A **28**, 2529 (1995).
[26] L. Benet, D. Trautmann, and T. H. Seligman, Celest. Mech. Dyn. Astron. **66**, 203 (1997); L. Benet, T. H. Seligman, and D. Trautmann, *ibid.* **71**, 167 (1998).
[27] P. Schlagheck and A. Buchleitner, Physica D **131**, 110 (1999); Phys. Rev. A **63**, 024701 (2001).